CHAPTER 2 LITERATURE REVIEW

2.1 Introduction

Nowadays, traffic factors such as heavier loads, higher traffic volume, and higher tire pressure are increasing. Therefore, distresses such as fatigue, rutting or thermal cracking of pavement are a main problem. A high performance pavement is required to mitigate this problem.

2.2 Flexible Pavements

Yoder and Witczak (1975) described types of pavement by dividing into two broad categories; flexible pavement and rigid pavement, as shown in Figure 2.1. Classical definitions of pavements, in some cases, represent an oversimplification. Pavement classification is subject to the limitations inherent to all classification techniques. In this study, flexible pavement is of interest.

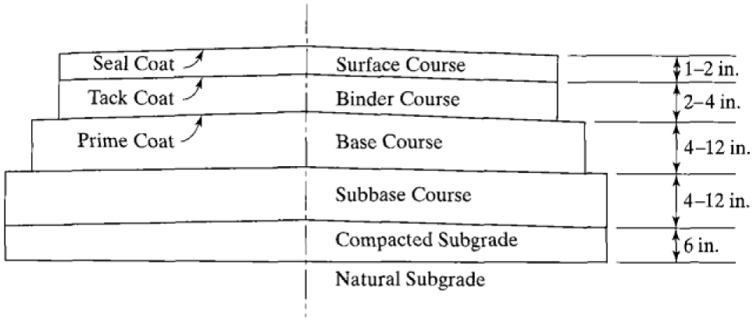

(a)

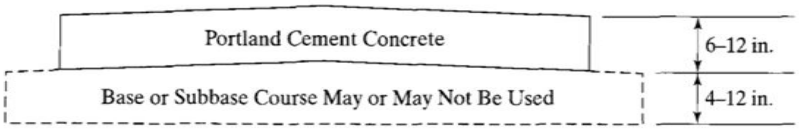

(b)

Figure 2.1 Characteristic of pavement: (a) flexible pavement and (b) rigid pavement (Huang, 2004)

2.2.1 Structure

2.2.1.1 Conventional flexible pavements

Conventional flexible pavements (asphaltic concrete) consist of multi layer. Each layer receives wheel loads from the overlying layer, distributes these loads in this layer, and passes on these loads to the underlying layer. So, stresses that it receives from wheel loads will be reduced. The stresses are maximum at the top layer and minimum at the lowest layer. This point is the major advantage of flexible pavements, because designers can use different materials in each layer. A material which has high load bearing capacity and the most expensive was used on the top layer, but a material which was used on the bottom has the lowest load bearing capacity and the least expensive (Huang, 2004).

AASHTO (1993) defined the flexible pavement structure as shown Figure 2.1(a). Starting from the top, the pavement consists of seal coat, surface course, tack coat, binder course, prime coat, base course, subbase course, compacted subgrade, and natural subgrade. The use of the various courses is based on either necessity or economy, and some of the course may be omitted. The meaning of each word is:

Seal Coat: Seal coat is a thin asphalt treatment used to waterproof the surface to provide skid resistance where the aggregates in the surface course could be polished by traffic and become slippery. Depending on the purpose, seal coats might or might not be covered with aggregate.

Surface Course: The surface course of a flexible structure consists of a mixture of mineral aggregates and bituminous materials placed as the upper course and usually constructed on the base course. In addition to its major function as a structural portion of the pavement, it must also be designed to resist the abrasive forces of traffic, to reduce the amount of surface water penetrating into the pavement, to provide a skid-resistance surface, and to provide a smooth and uniform riding surface.

Binder course: The binder course, sometimes called the asphalt base course, is the asphalt layer below the surface course. There are two reasons that a binder course is used in addition to the surface course. First, the hot-mixed asphaltic (HMA) is too thick to be compacted in one layer, so it must be placed in two layers. Second, the binder course generally consists of larger aggregates and less asphalt and does not require as high a quality as the surface course, so replacing a part of the surface course by the binder course results in a more economical design. If the binder course is more than 3 in. (76 mm), it is generally placed in two layers.

Tack Coat and Prime Coat: A tack coat is a very light application of asphalt, usually asphalt emulsion diluted with water, used to ensure a bond between the surface being paved and the overlaying course. It is important that each layer in an asphalt pavement be bonded to the layer below. Tack coats are also used to bound the asphalt layer to a PCC base or an old asphalt pavement. The three essential requirements of a tack coat are that it must be very thin, it must uniformly cover the entire surface to be paved, and it must be allowed to break or cure before the HMA is laid.

A prime coat is an application of low-viscosity cutback asphalt to an absorbent surface, such as an untreated granular base on which an asphalt layer will be placed. Its purpose is to bind the granular base to the asphalt layer. The difference between a tack coat and a prime coat is that a tack coat does not require the penetration of asphalt into the underlying layer, whereas a prime coat penetrates into the underlying layer, plugs the voids, and forms a watertight surface. Although the type and quantity of asphalt used are quite different, both are spray applications.

***Base Course*:** The base course is the portion of the pavement structure immediately beneath the surface course and it is constructed on the subbase course. Its major function in the pavement is structural support and usually consists of aggregates: e.g., crushed stone, crushed slag, crushed gravel and sand, or combinations of these materials. Specifications for base course are generally considerably more stringent than the one for subbase materials in requirements for strength, plasticity, and gradation.

***Subbase Course*:** The subbase course is the portion of the flexible pavement structure between the roadbed soil and the base course. It usually consists of a compacted layer of granular material, either treated or untreated. In addition to its position in the pavement, it is usually distinguished from the base course material by less stringent specification requirements for strength, plasticity, and gradation. The subbase material should be of significantly better quality than the roadbed soil.

***Subgrade*:** The subgrade is the lowermost material placed in the flexible pavement structure or placed on unmoved soil from cuts in the normal grading of the roadbed. It is the foundation for the flexible pavement structure. Sometimes, we called the subgrade as Foundation Soil or Roadbed Soil (AI, 1986).

2.2.1.2 Full-depth asphalt pavements

Full-depth asphalt pavements are constructed by placing one or more layers of hot-mixed asphaltic (HMA) directly on the subgrade or improved subgrade. This concept was conceived by the Asphalt Institute (AI, 1960) and is generally considered the most cost-effective and dependable type of asphalt pavement for heavy traffic. This type of construction is quite popular in areas where local materials are not available. It is more convenient to purchase only one material, i.e., HMA rather than several materials from different sources, thus minimizing the administration and equipment costs.

Figure 2.2 shows the typical cross section for a full-depth asphalt pavement. The asphalt base course in the full-depth construction is the same as the binder course in conventional pavement. As with conventional pavement, a tack coat must be applied between two asphalt layers to bind them together.

According to the Asphalt Institute (AI, 1987), full-depth asphalt pavement have the following advantages;

1. They have no permeable granular layers to entrap water and impair performance.
2. Time required for construction is reduced. On widening projects, where adjacent traffic flow must usually be maintained, full-depth asphalt can be especially advantageous.
3. When placed in a thick lift of 4 in. (102 mm) or more, construction seasons may be extended.
4. They provide and retain uniformity in the pavement structure.
5. They are less affected by moisture or frost.
6. According to limited studies, moisture contents do not build up in subgrades under full-depth asphalt pavement structures as they do under pavements with granular bases. Thus, there is little or no reduction in subgrade strength.

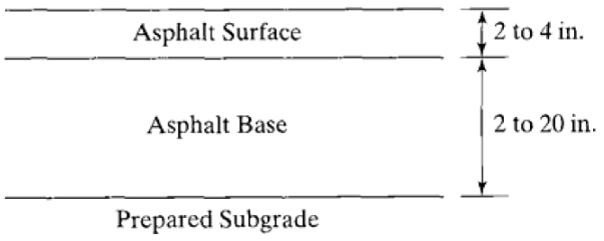

Figure 2.2 Characteristic of full-depth asphalt pavement (Huang, 2004)

2.2.2 Design factors

The design factors can be broadly separated into four categories; traffic and loading, environment, materials, and failure criteria. (Huang, 2004):

2.2.2.1 Traffic and Loading

The traffic and loading to be considered include axle loads, the number of load repetitions, tire contact areas, and vehicle speeds.

Axle Loads: Figure 2.3 shows the wheel spacing for a typical semitrailer consisting of single axle with single tires, single axle with dual tires, and tandem axles with dual tires. In the design of flexible pavements by layered theory, only the wheels on one side, say at the outer wheelpath, need be considered.

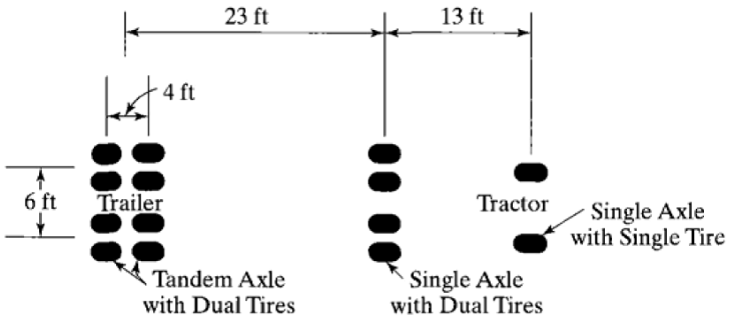

Figure 2.3 Wheel configurations for typical semitrailer units (Huang, 2004)

Number of Repetitions: With the use of a high-speed computer, it is no problem to consider the number of load repetitions for each axle load and evaluate its damage. Instead of analyzing the stresses and strains due to each axle-load group, a simplified and widely accepted procedure is to develop equivalent factors and convert each load group into an equivalent 18-kip (80-kN) single-axle load, as illustrated by the Asphalt Institute method (AI, 1991) and the AASHTO method (AASHTO, 1986).

Contact Area: In the mechanistic method of design, it is necessary to know the contact area between tire and pavement, so the axle load can be assumed to be uniformly distributed over the contact area.

Vehicle Speed: Another factor related to traffic is the speed of traveling vehicles, such as speed is directly related to the duration of loading.

2.2.2.2 Environment

The environmental factors that influence pavement design include temperature and precipitation.

Temperature: The temperature affects the resilient modulus of asphalt layers. In cold climates, the resilient moduli of unstabilized materials also vary with the freeze–thaw cycles. The severity of cold climate is indicated by the freezing index, which can be correlated with the depth of frost penetration.

Precipitation: The precipitation from rain and snow affects the quantity of surface water infiltrating into the subgrade and the location of the groundwater table. Every effort should be made to improve drainage and alleviate the detrimental effect of water. If water from rainfalls can be drained out within a short time, its effect can be minimized, even in regions of high precipitation. The location of the groundwater table is also important. The water table should be kept at least 3 ft (0.91 m) below the pavement surface. In seasonal frost areas, the depth from the pavement surface to the groundwater table should be much greater.

2.2.2.3 Materials

In the mechanistic-empirical methods of design, the properties of materials must be specified, so that the responses of the pavement, such as stresses, strains, and displacements in the critical components, can be determined. These responses are then used with the failure criteria to predict whether failures will occur or the probability that failures will occur.

2.2.2.4 Failure Criteria

One of the important design factors to be considered is the failure criteria. It is generally agreed that fatigue cracking, rutting, and thermal cracking are the three principal types of distress to be considered for flexible pavement design.

2.3 Flexible Pavement Distress

2.3.1 Fatigue Cracking

The fatigue cracking of flexible pavements is based on the horizontal tensile strain at the bottom of HMA. The failure criterion relates the allowable number of load repetitions to the tensile strain, through the laboratory fatigue test on small HMA specimens. The difference in geometric and loading conditions makes the allowable number of repetitions for actual pavements much greater than that obtained from laboratory tests. Therefore, the failure criterion must incorporate a shift factor to account for the difference (Huang, 2004).

2.3.1.1 Severity Levels

Severity level of fatigue cracking is separated to 3 levels; low, moderate and high (Miller and Bellinger, 2003). The detail of each level is explained below (Figure 2.4):

Low: An area of cracks with no or only a few connecting cracks; cracks are not spalled or sealed; pumping is not evident.

Moderate: An area of interconnected cracks forming a complete pattern; cracks may be slightly spalled; cracks may be sealed; pumping is not evident.

High: An area of moderately or severely spalled interconnected cracks forming a complete pattern; pieces may move when subjected to traffic; cracks may be sealed; pumping may be evident.

If different severity levels existing within an area cannot be distinguished, rate the entire area at the highest severity present.

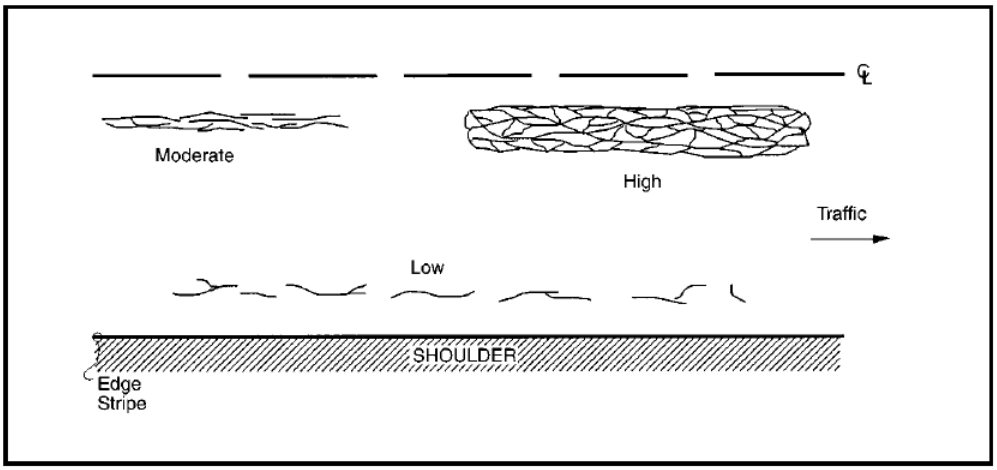

(a)

(b)

Figure 2.4 Fatigue cracking: (a) severity level and (b) characteristic (Miller and Bellinger, 2003)

2.3.2 Rutting

Rutting (Figure 2.5) is occurred only on flexible pavements. Pavement uplift (shearing) may occur along the sides of the rut. Ruts are particularly evident after a rain when they are filled with water. There are two basic types of rutting: mix rutting and subgrade rutting. Mix rutting occurs when the subgrade does not rut yet the pavement surface exhibits wheelpath depressions as a result of compaction/mix design problems. Subgrade rutting occurs when the subgrade exhibits wheelpath depressions due to loading. In this case, the pavement settles into the subgrade ruts causing surface depressions in the wheelpath (Muench, 2005).

Severity level of rutting is not applicable. Severity levels could be defined by categorizing the measurements taken. A record of the measurements taken is much more desirable, because it is more accurate and repeatable than are severity levels (Miller and Bellinger, 2003).

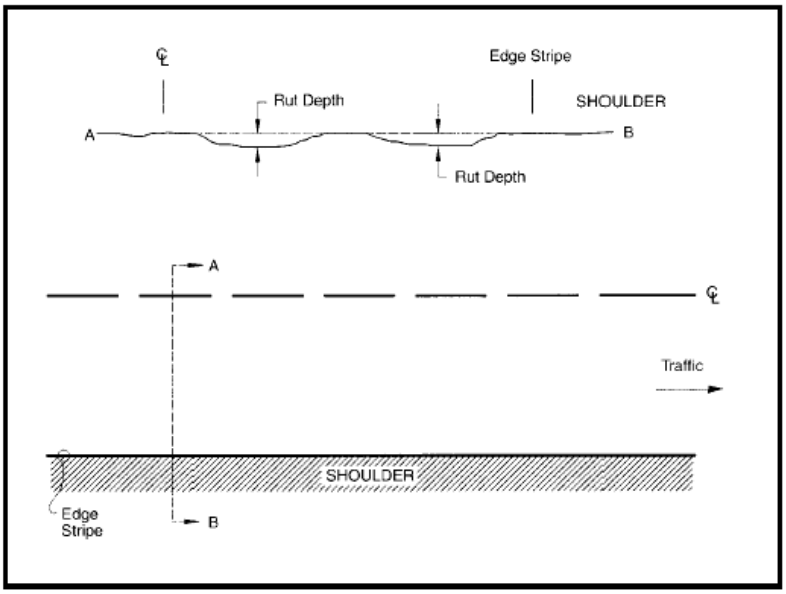

(a)

(b)

Figure 2.5 Rutting: (a) and (b) characteristic (Miller and Bellinger, 2003)

2.3.3 Thermal Cracking

Cracks are predominantly perpendicular to pavement centerline. This type of distress includes both low-temperature cracking and thermal fatigue cracking. Low-temperature cracking is usually associated with flexible pavements in northern regions of the United States and much of Canada, where winter temperatures can fall below -10 °F(-23 °C) . Thermal fatigue cracking can occur in much milder regions if excessively hard asphalt is used or the asphalt becomes hardened by aging. Thermal fatigue cracking is similar to the fatigue cracking caused by repeated loads. It is caused by the tensile strain in the asphalt layer that is due to daily temperature cycle (Huang, 2004).

2.3.3.1 Severity Levels

Severity level of thermal cracking is separated to 3 levels; low, moderate and high (Miller and Bellinger, 2003). The detail of each level is explained below (Figure 2.6):

Low: An unsealed crack with a mean width ≤ 6 mm; or a sealed crack with sealant material in good condition and with a width that cannot be determined.

Moderate: Any crack with a mean width > 6 mm and ≤ 19 mm; or any crack with a mean width ≤ 19 mm and adjacent low severity random cracking.

High: Any crack with a mean width > 19 mm; or any crack with a mean width ≤ 19 mm and adjacent moderate to high severity random cracking.

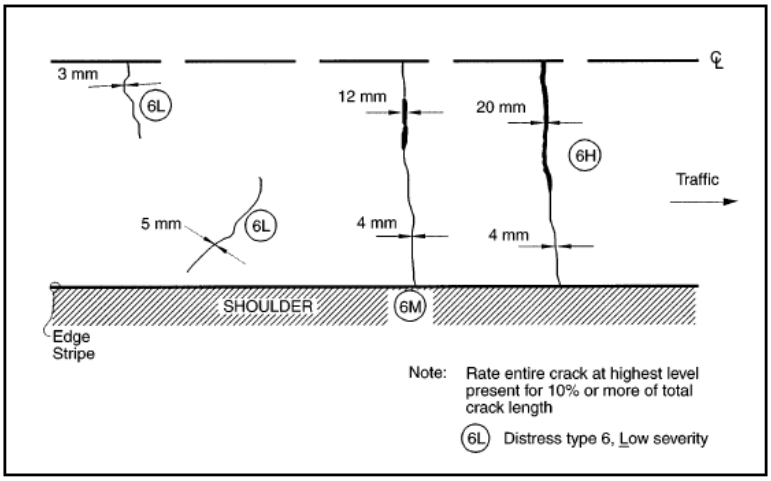

(a)

(b)

Figure 2.6 Thermal cracking: (a) severity level and (b) characteristic (Miller and Bellinger, 2003)

2.4 Flexible Pavement Improvement

The flexible pavements have been exposed to greater stresses because of the increasing traffic volumes, truck traffic and higher tire pressures. Thus, the high performance pavement is required for increasing stress capacity. For this study, there are 2 interesting alternatives for this purpose; 1) improvement of pavement material by replacing AC 60 – 70 with polymer-modified asphalt cement (PM -AC) in preparation of pavement , and 2) use of geosynthetic reinforcement for reinforcing the pavement material.

2.4.1 Polymer Modified Asphalt Cement (PM-AC)

A high performance pavement requires asphalt cement that is less susceptible to high temperature rutting, fatigue cracking or low temperature cracking and has excellent adherence to stone aggregates. Mixing a polymer with the asphalt has potential for addressing the distress problems that exist in today's highways. Polymer modification typically improves binder ductility, thereby providing a binder that is more durable to pavement stress and deformation, due to, e.g., low temperature thermal contraction or traffic loads, including the effects of fatigue. Finally, there is evidence that polymer modifiers may improve the aging characteristics of a binder so that the deleterious impact of oxidative aging is delayed, leading to a more durable pavement (Glover et al., 2005).

2.4.1.1 Methods for incorporate polymer into asphalt

Two methods are commonly used to incorporate polymers into asphalt (Becker et al., 2001);

- Addition of latex polymer to the asphalt. This method is relatively easy and trouble free.
- Addition of solid polymers to asphalt. This method normally requires substantial mixing and shearing in order to uniformly disperse the polymers.

2.4.1.2 Types of Polymer Modifiers

Two basic types of polymer are used in modifying bitumen for road applications; elastomer and plastomer (Johnston and King, 2008). An elastomer is a polymer that has a flexible 'rubber' backbone and large side-chains in its structure. Styrene butadiene styrene (SBS) is an example of this type. A plastomer is a polymer that will deform in a plastic or viscous manner at melt temperatures and becomes hard and stiff at low temperatures, i.e. the structure is reversibly broken down with the application of heat. An example of such a material is ethylene vinyl acetate (EVA) (BP, 2001).

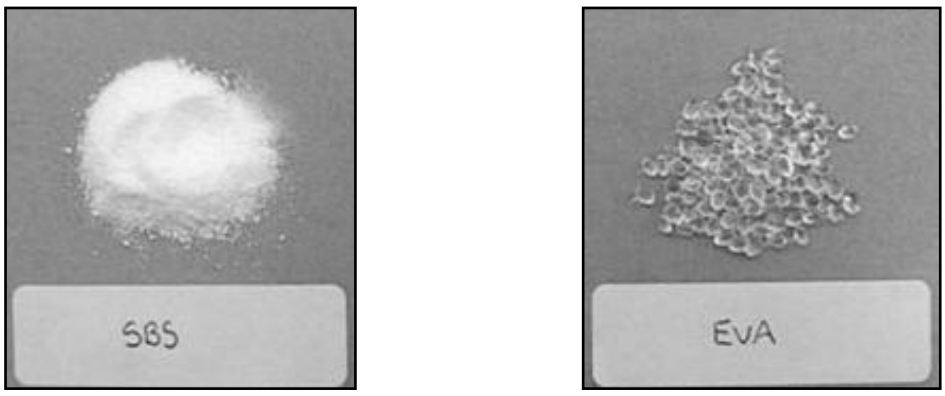

(a) (b)

Figure 2.7 Examples of different polymers: (a) styrene butadiene styrene (SBS); and (b) ethylene vinyl acetate (EVA) (Robinson, 2011)

Currently, the most commonly used polymer for bitumen modification is the styrene butadiene styrene (SBS) followed by other polymers such as styrene butadiene rubber (SBR), ethylene vinyl acetate (EVA) and polyethylene (Airey, 2004). Styrene butadiene styrene (SB, SBS) mixtures have shown the highest resistance to the permanent deformation and harmonious results are concerned with the repeated creep tests (Figure 2.8) when comparing with polialfaolefin (AP), cellulosed fiber (SE), cellulosed fiber mixed with bitumen (BE) and polyolefin (PE) mixtures (Tayfur et al., 2005).

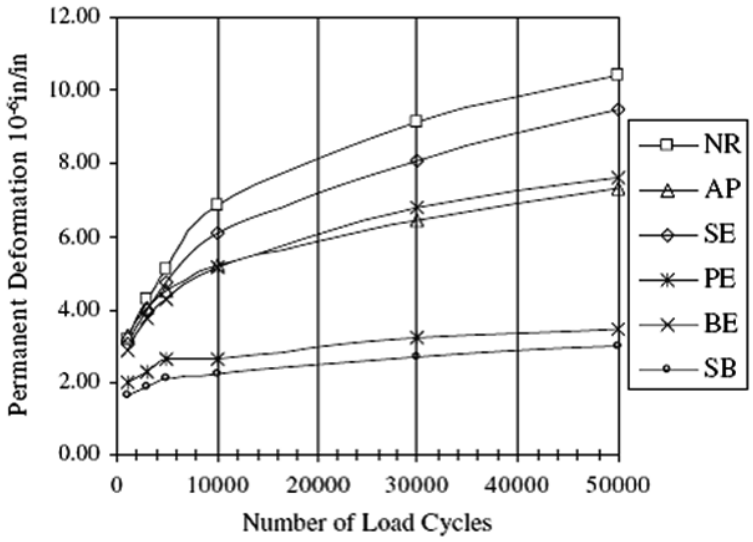

Figure 2.8 LCPC wheel test result (Tayfur et al., 2005)

Sengoz and Isikyakar (2007) presented a laboratory study of modified bitumen containing styrene–butadiene–styrene (SBS) and ethylene vinyl acetate (EVA) copolymers and a 50/70 penetration grade base. The results indicated that, SBS bitumen has shown a greater degree of improvement in modification compared to EVA bitumen with differences being more pronounced at higher polymer contents, as shown in Figure 2.9.

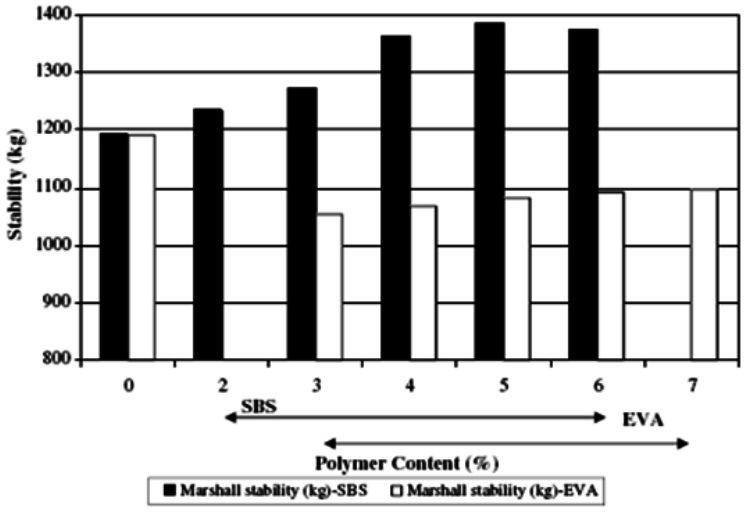

Figure 2.9 Marshall stability value of polymer modified HMA (Sengoz and Isikyakar, 2007)

2.4.1.3 Content of Polymer Modifiers

The phase morphology of the polymer modified bitumens is the result of the mutual effects of polymer and bitumen and is influenced by polymer content. The formation of a continuous SBS polymer phase is dependent on SBS polymer content, as shown in Figure 2.10. For these particular materials, phase inversion from a continuous bitumen phase to continuous SBS polymer phase occurs when SBS content is around 5%. This content can be accepted as intertwisted phase which is an ideal microstructure for polymer modified road asphalt. From indirect tensile strength test, SBS mixture, which the content is 5%, showed the highest indirect tensile strength, as shown in Figure 2.11 (Sengoz and Isikyakar, 2007).

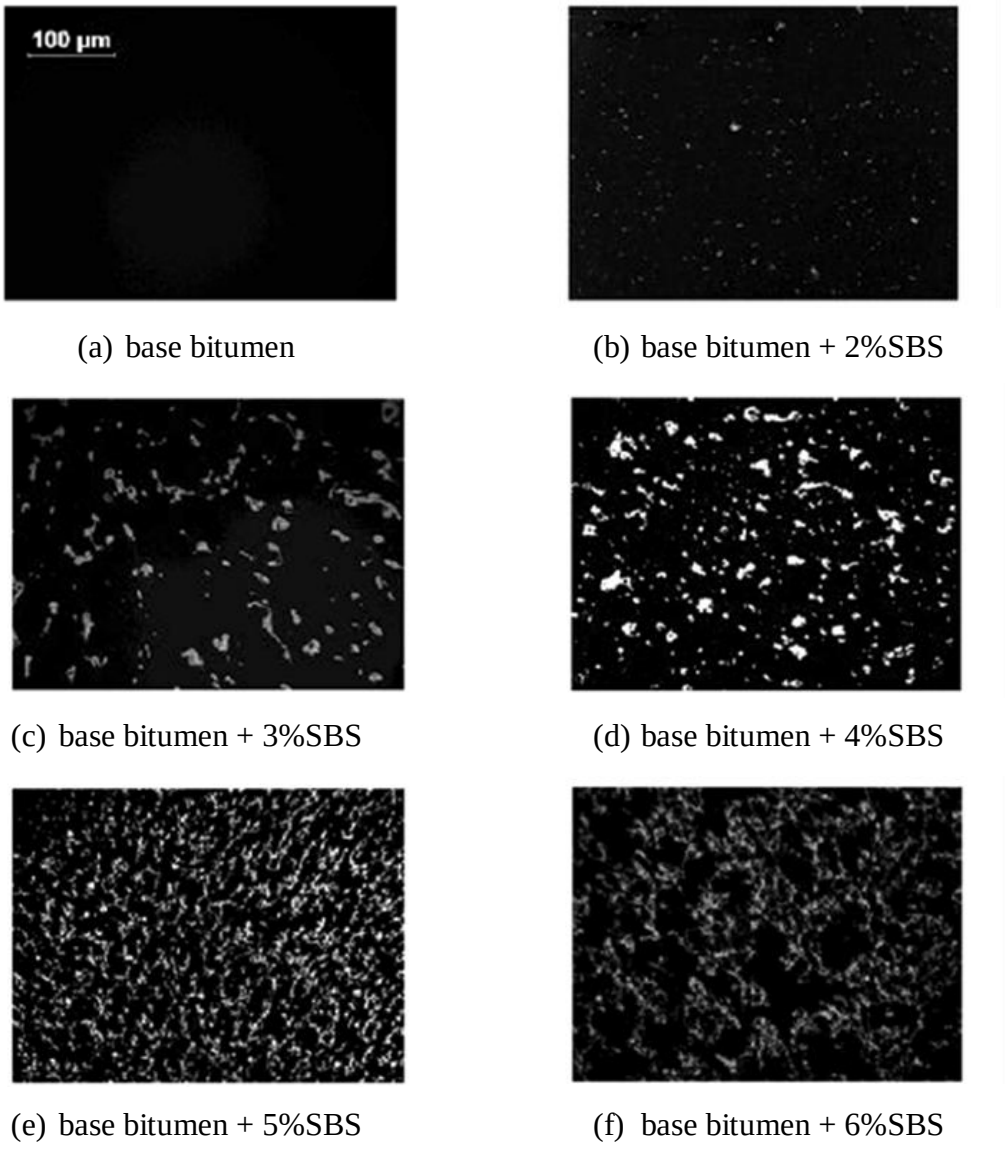

(a) base bitumen (b) base bitumen + 2%SBS

(c) base bitumen + 3%SBS (d) base bitumen + 4%SBS

(e) base bitumen + 5%SBS (f) base bitumen + 6%SBS

Figure 2.10 Fluorescent images of SBS PMB samples with 100x magnification (Sengoz and Isikyakar, 2007)

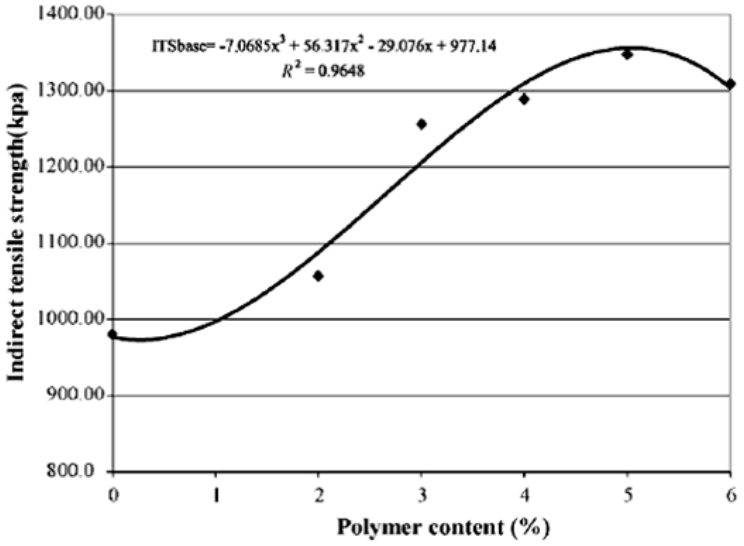

Figure 2.11 Indirect tensile strength values of polymer modified HMA (Sengoz and Isikyakar, 2007)

2.4.1.4 Fatigue Cracking Resistance

From investigation of the utilizing a polyester resin for reinforcing flexible pavements, the reinforcement was effective in reducing the stiffness of the mixture whilst improving load-carrying capacity. The effect of the polymer coating was extended to a significant improvement in the resistance to crack propagation, approximately 2.5 times the load cycle of a normal mixture without reinforcement (Kim et al., 1996).

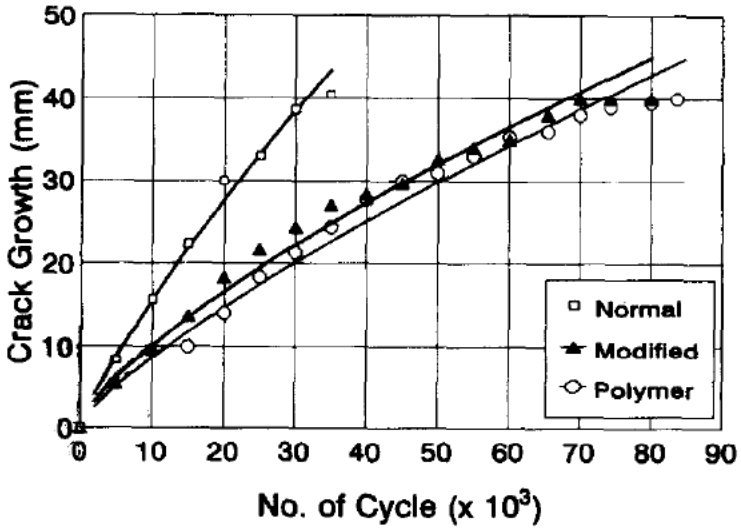

Figure 2.12 Crack propagation by number of load cycles (Kim et al., 1996)

Sengoz and Isikyakar (2007) presented a laboratory study of modified bitumen containing styrene-butadiene-styrene (SBS) copolymer. SBS modification increases in softening point, reduces in penetration, increases stiffness (hardness) of the Polymer Modified Bitumens (PMBs). PMBs may be less sensitive to permanent deformation. It is possible to consider that SBS polymer addition minimizes the pavement deficiencies revealed due to aging, thus providing an increase in the service life of the road.

2.4.1.5 Rutting Resistance

Polymer modification has been increasingly employed in asphalt concrete, primarily for control of short-term permanent deformation (rutting) (Bouldin and Collins, 1992; Isacsson and Lu, 1995).

Chen et al. (2002) reported the development of a procedure to evaluate and optimize a polymer modified asphalt (PMA). Rut depth decreases with increasing polymer percentages, as indicated in Figure 2.13. The most significant reduction of rutting occurs at the addition of 6% SBS. Adding more than 6% SBS may not be economically feasible, however, because of the limited effect on rutting reduction.

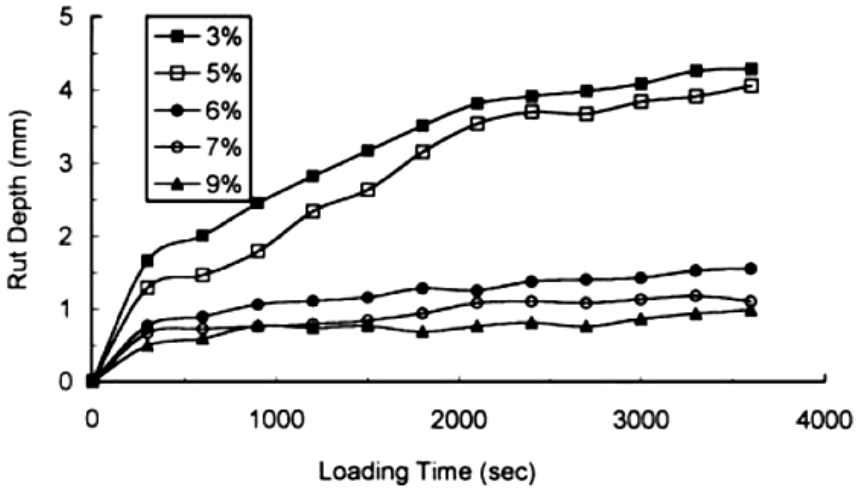

Figure 2.13 Rut depth obtained from the wheel-tracking test (Chen et al., 2002)

2.4.1.6 Thermal Cracking Resistance

A thermal stress restrained specimen test (TSRST) was performed on polymer-modified asphalt with regard to low temperature behavior (Isacsson and Zeng, 1996). Based on the results obtained, the additions of polymers to bitumens increase the resistance to low-temperature cracking of asphalt pavements.

Low-temperature properties of the modified bitumens containing styrene butadiene styrene (SBS) were investigated using conventional methods, dynamic mechanical analysis (DMA) and bending beam rheometer (BBR). The results indicated that SBS polymers improved low-temperature properties of bitumens. The polymer modification reduces the creep stiffness and limiting stiffness temperature of bitumens (Lu et al., 1998).

The lap-shear test was used to study the interfacial adhesion and behavior between polymer modified asphalts (AC5-SBS and AC10-SBS) and aggregate. At lower temperatures, the lap-shear strength of modified mixtures was higher than those of unmodified mixtures and they increased with increasing polymer (Khattak et al., 2007).

2.4.2 Geosynthetics

Geosynthetics can be defined as planar products manufactured from polymeric material, which are used with soil, rock, or other geotechnical-engineering-related material as an integral part of a synthetic project, structure, or system (ASTM, 1995). Geosynthetics are widely used in many geotechnical and transportation applications.

2.4.2.1 Types of Geosynthetics

There are eight types of geosynthetics (Figure 2.14): 1) geotextiled, 2) geogrids, 3) geonets, 4) geomembranes, 5) geosynthetic clay liners, 6) geopipe, 7) geofoam, and 8) geocomposites (Koerner, 2005). Description of each type is shown below.

Geotextiles: They can be classified as woven, nonwoven, or knitted. Woven fabrics exhibit high tensile strength, high modulus, and low strains, while nonwoven fabrics have high permeability and high strain characteristics. Geotextiles are manufactured in a variety of geometric and polymeric compositions to meet a number of different applications. Many geotextiles are made of polypropylene (PTA, 2005).

Geogrids: Geogrids have a uniformly distributed array of apertures between their longitudinal and transverse elements. The apertures allow direct contact between soil particles on either side of the installed sheet, thereby increasing the interaction between the geogrid and the backfill soil. Geogrids are composed of polypropylene, polyethylene, polyester, or coated polyester (Zornberg et al., 2008).

Geonets: Geonets are formed by a continuous extrusion of parallel sets of polymeric ribs at acute angles to one another. When the ribs are opened, relatively large apertures are formed into a netlike configuration. Their design function is completely within the drainage area where they are used to convey liquids of all types (Koerner, 2005).

Geomembranes: The materials themselves are relatively thin, impervious sheets of polymeric material used primarily for linings and covers of liquid or solid storage facilities. This includes all types of landfills, reservoirs, canals, and other containment facilities. Thus the primary is always containment as a liquid or vapor barrier or both (Koerner, 2005).

Geosynthetic Clay Liners: Geosynthetic Clay Liners (GCLs) are geocomposites that are prefabricated with a bentonite clay layer typically incorporated between a top and bottom geotextile layer or bonded to a geomembrane or single layer of geotextile. Geotextile-encased GCLs are often stitched or needle-punched through the bentonite core to increase internal shear resistance (Bathurst, 2006).

Geopipe: Geopipe are perforated or solid-wall polymeric pipes used for drainage of liquids or gas (including leachate or gas collection in landfill applications). In some cases, the perforated pipe is wrapped with a geotextile filter (Bathurst, 2006).

Geofoam: Geofoam refers to low-density cellular plastic foam, either molded expanded polystyrene blocks or extruded polystyrene sheets. Geofoam is used as a super lightweight fill, with 1.5 to 3.0 pounds per cubic foot density. Geofoam's light weight makes it a viable option for landslide repair and for embankments on soft,

compressible deposits. Geofoam is also used for thermal insulation of pavements and foundations (PTA, 2005).

Geocomposites: Geocomposites are designed to replace aggregate and/or perforated pipe subsurface drainage systems. A geocomposite consists of a deformed, perforated, or slotted plastic core and a geotextile (filter) fabric wrap. Geocomposites include geonets, pavement edge drains (drainage mats), and sheet (wall) drains. Wick (strip) drains, used to expedite drainage of deep, compressible soil deposits, have also been included in the geocomposite category. The core material could be HDPE, polypropylene, polyvinyl chloride (PVC), high impact polystyrene, or a combination of two polymers (PTA, 2005).

(a) (b)

(c) (d)

(e) (f)

Figure 2.14 Geosynthetics: (a) Geotextiles, (b) Geogrids, (c) Geonets, (d) Geomembranes, (e) Geosynthetic Clay Liners, (f) Geopipe, (g) Geofoam and (h) Geocomposites (NAGS, 2011 and Koerner, 2006)

(g)

(h)

Figure 2.14(Cont.) Geosynthetics: (a) Geotextiles, (b) Geogrids, (c) Geonets, (d) Geomembranes, (e) Geosynthetic Clay Liners, (f) Geopipe, (g) Geofoam and (h) Geocomposites (NAGS, 2011 and Koerner, 2006)

2.4.2.2 Reinforced Pavements

Reinforcing is a structural measure to increase the strength. Reinforcing road pavement is concerned with increasing pavement resistance to a variety of stresses and improving its strength characteristics. When reinforcing pavement by geosynthetics, the rheological model of asphalt pavement changes (Laurinavičius and Oginskas, 2006).

The performances of geosynthetic-reinforced asphalt pavement under monotonic, cyclic, and dynamic loading are studied in laboratory (Ling and Liu, 2001). Two different types of geogrid layer were installed at the bottom of the asphalt concrete layer, along the asphalt-subgrade interface, to function as tensile reinforcement, as shown in Figure 2.15. The load was applied to the surface of the asphalt concrete layer using a rigid rectangular footing under plane strain conditions. The results of static and dynamic loading tests indicated that the geosynthetic reinforcement contributed to an improvement in the stiffness (slope of load versus settlement relationships) and strength of asphalt pavement (Figures 2.16 and 2.17). The settlement over the loading area of reinforced pavement was reduced when compared with unreinforced pavement. The test results also showed that the bonding between geosynthetic reinforcement and asphalt and the stiffness of geogrid ensured a satisfactory performance.

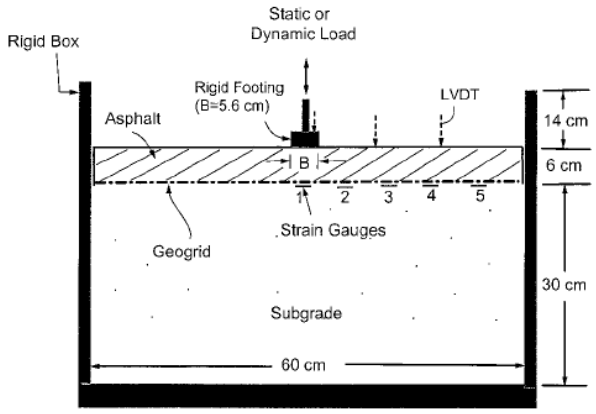

Figure 2.15 Experimental set up of a physical model test on reinforced pavement (Ling and Liu, 2001)

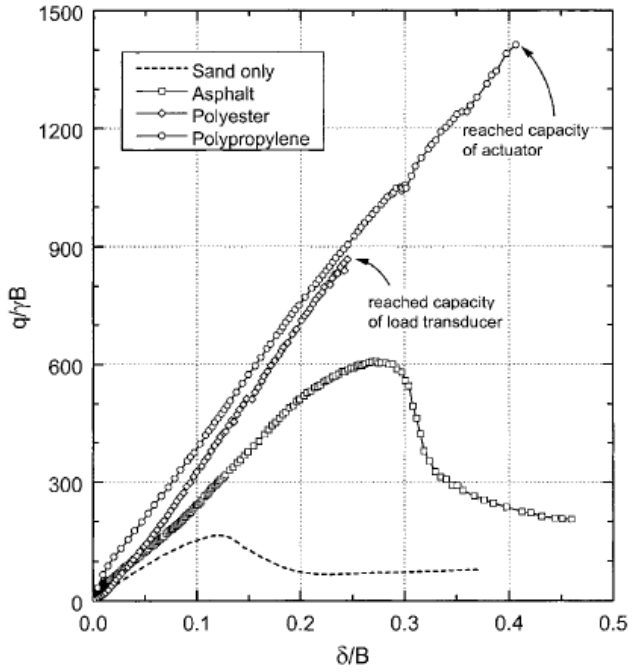

Figure 2.16 Load-Settlement Relationships of Unreinforced and Reinforced Asphalt Concrete Pavement: Monotonic Loading (Ling and Liu, 2001)

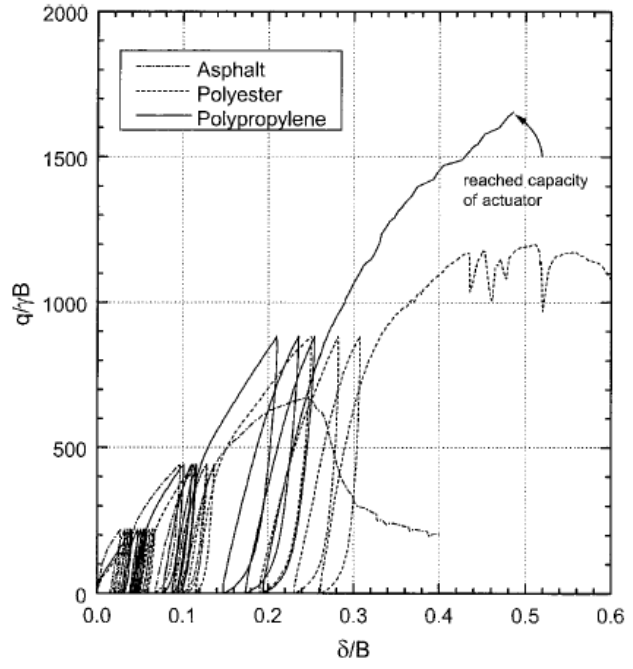

Figure 2.17 Load-Strain Relationships of Unreinforced and Reinforced Asphalt Concrete Pavement: Cyclic Loading (Ling and Liu, 2001)

Scaled-down physical model test on reinforced flexible pavement structure were performed (Thaisri, 2007, Kunakulsawat et al., 2010 and Youwai et al., 2010). The physical model was prepared by pluviating through air a cleaned uniform sand (KMUTT sand) as base layer. Then, a 6-cm thick asphaltic concrete (AC) layer, either unreinforced or reinforced with different types of geosynthetic reinforcement as well as their combination and arrangement, was place on the top surface of the sand layer. The AC layer was compressed repeatedly for 200 cycles by means of a 6-cm wide rigid rough footing placed at the center. The average footing settlements as well as deflections along the lengthwise of AC layer were measured. In addition, strain fields of sand layer were computed by a photogrammetric analysis. When considering the footing settlement, it was found that the permanent deformation of AC layer decreased when reinforced with geosynthetic (Figure 2.18). And, when the number of cycles of cyclic loading increased, the footing settlement increased but it was at decreasing rate. This is due to that the rigidity of AC layer increased when being reinforced. Therefore, the stress activated on the top surface of AC layer via footing can be effectively distributed to materials located below at a much wider area. Then, the maximum shear strain distribution of the based layer was uniformly distributed with the average value that was lower than the one when unreinforced (Figure 2.19).

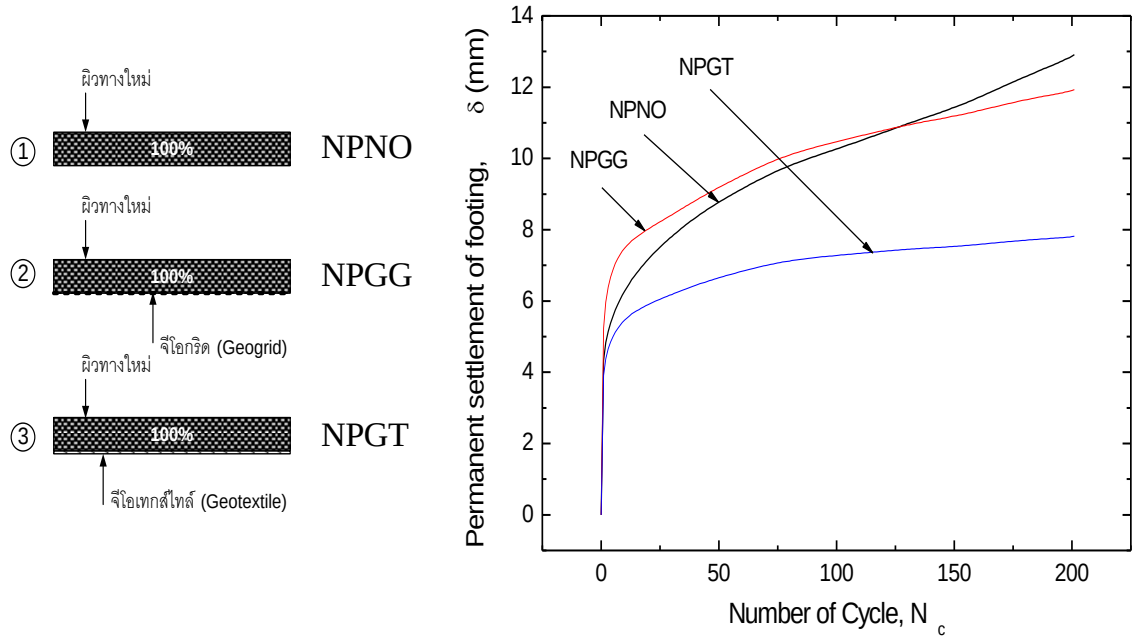

Figure 2.18 Permanent settlement-Number of cycle Relationships of New Unreinforced and Reinforced Asphalt Concrete Pavement (Thaisri, 2007)

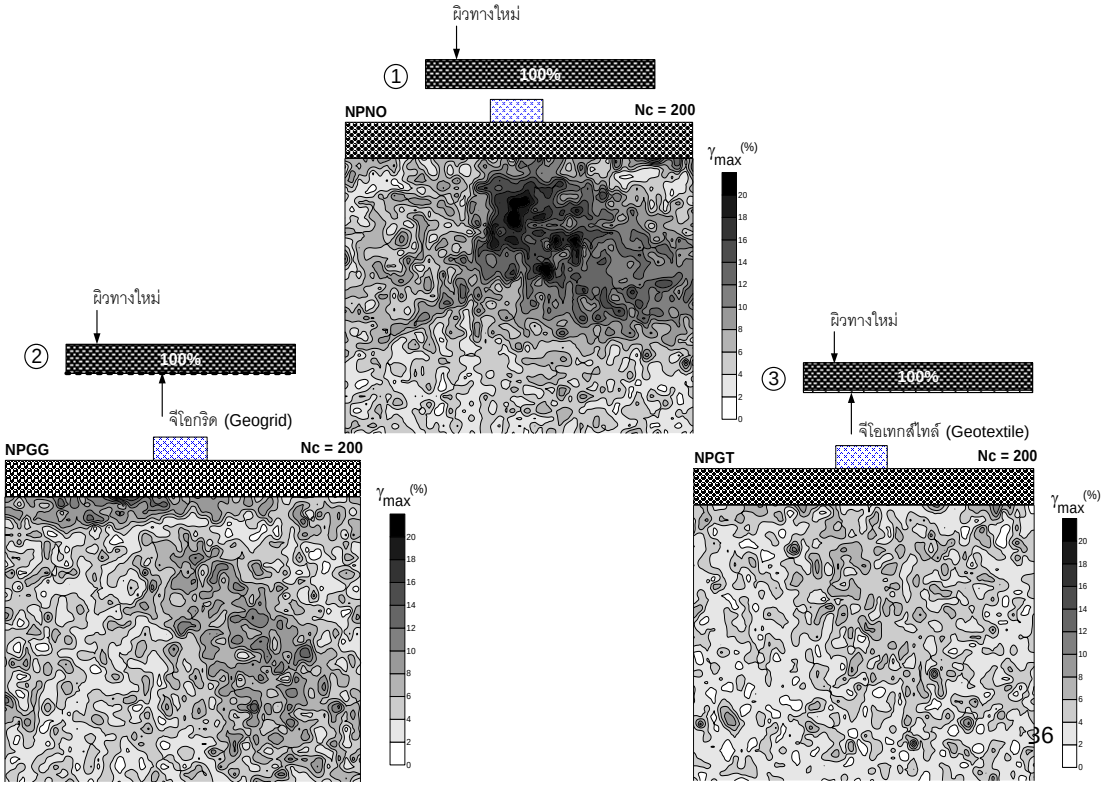

Figure 2.19 Strain fields of New Unreinforced and Reinforced Asphalt Concrete Pavement (Thaisri, 2007)

A fabric effectiveness factor (FEF) can be used and implemented into the design traffic number to determine a modified value and design accordingly, that is

$$FEF = \frac{DTN_N}{DTN_R} \tag{2.1}$$

where: DTN_R = Design traffic number for the reinforced case

DTN_N = Design traffic number under standard (nonreinforced) conditions (e.g., using the Asphalt Institute's procedures) (Koerner, 2005)

2.4.2.3 Effect of Location of Geosynthetics

The performance of geogrid base reinforcement in flexible pavements was evaluated using cyclic plate load testing. The investigated parameters included location of geogrids (Abu-Farsakh and Chen, 2011). The effect of geogrid location was investigated by using GG3 and GG4 geogrids. The following reinforcement locations; placing geogrid at the base–subgrade interface, placing geogrid at the middle of the base layer and placing geogrid at the upper one-third of the base layer. The Best performance was observed when geogrid layer was placed at the upper one-third of the base aggregate layer (Figure 2.20).

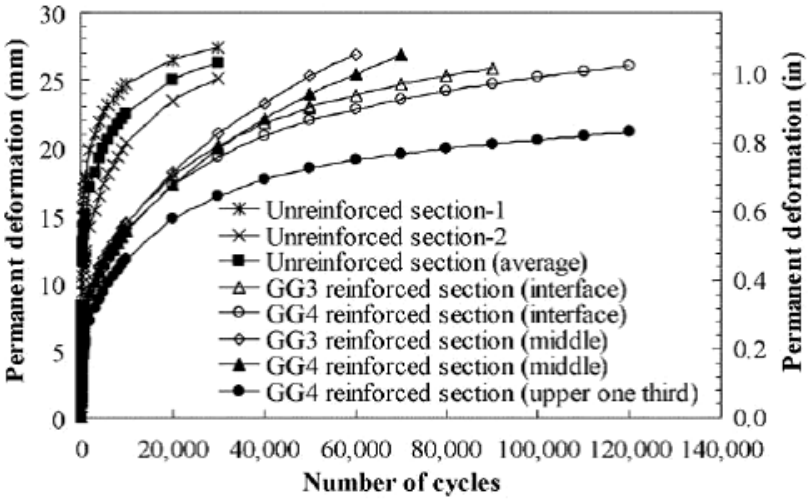

Figure 2.20 Development of surface permanent deformation for different types of GG3 and GG4 geogrids placed at different locations (Abu-Farsakh and Chen, 2011)

2.5 Flexible Pavements Rehabilitation

The combined effects of traffic loading and the environment will cause pavements to deteriorate over time. Although maintenance can slow the rate of deterioration, it cannot stop it. Therefore eventually the effects of deterioration need to be reversed by adding or replacing material in the existing pavement structure. This is called rehabilitation. Formally, rehabilitation can be defined as a structural or functional enhancement of a pavement which produces a substantial extension in service life, by substantially improving pavement structurally and functionally (Tuna, 2006).

2.5.1 Types of Rehabilitation

Flexible pavement rehabilitation methods depend upon local conditions and pavement distress types but typically include (Lenz, 2011); in-place surface recycling, geosynthetics, flexible base overlay and flexible base thickening, full depth reclamation/recycling (FDR), HMA overlays, surface treatments, concrete overlays, and other options.

In-Place Surface Recycling: There are two types of this method; hot in-place recycling (HIPR), and cold in-place recycling (CIR). The HIPR process involves recycling the existing asphalt surface layer by heating, scarifying, and adding a recycling agent, but the CIR process treatments the existing asphalt pavements without heating.

Geosynthetics: Geosynthetics can be part of an overall rehabilitation strategy that will, as a minimum, include the placement of a new wearing/surface course of hot-mixed asphaltic (HMA). In this study, this procedure is of interest.

Flexible Base Overlay and Flexible Base Thickening: The flexible base overlay has been used as an intermediate layer of a new structure, placed directly on top of an old structure for resist the propagation of reflective cracks from the old structure. The flexible base thickening can be used to improve the structural capacity of low to

moderate volume highways. This technique can be used where there are low levels of existing structural damage, the existing base is uniform and the subgrade offers good support.

Full Depth Reclamation/Recycling (FDR): This rehabilitation procedure entails pulverizing the old pavement structure, blending in a stabilizing agent, compacting, adding additional material, and resurfacing.

HMA Overlays: Structural overlays are designed to add structural support to the existing pavement. Because of this, they are structurally designed and are thicker than non-structural overlays. In this study, this procedure is of interest.

Surface Treatments: Surface treatments are applied to restore texture and weatherproofing (including protection from oxidation), but do not contribute to improvement in ride or increas structural capacity.

Concrete Overlays: Applying a concrete overlay on a HMA surfaced pavement may be a viable rehabilitation strategy under certain circumstances. Where existing distress in an HMA-surfaced structure is confined to the HMA itself (mix rutting, shoving, wash boarding, cracking), but otherwise the existing substructure is sound, a concrete overlay can offer a durable replacement surface.

2.5.2 Geosynthetics Reinforced in HMA Overlays Pavement

Laboratory testing (i.e., wheel tracking test, scaled-down physical model test and four point beam test) is typically used because test sections can be constructed and tested relatively quickly, permitting multiple alternatives to be evaluated. The wheel tracking test is used for investigation the geogrid-reinforced asphalt concrete (Komatsu et al., 1998). The geogrid-reinforced asphalt concrete showed remarkable increases in the durability in comparison with the control without geogrids. This was because the stress concentration applied by a wheel load was greatly reduced by the high stiffness and small meshes of the thin geogrid inserted in the asphalt concrete.

The scaled-down geosynthetic-reinforced pavement was set, as shown in Figure 2.21 by Laurinavičius and Oginskas (2006) for exploring the development of shear strains and rutting in asphalt pavement as well as to suggest and describe the main methods for reducing the deformation. From the result, the rutting depth increases from 1.4 to 2.2 times with geosynthetic materials and 3 times without a geosynthetic material. Also, geosynthetics has been used to decrease shear strains in asphalt concrete layers. The accomplished research into reinforced asphalt concrete has established that the rutting depth depends on the type of geosynthetic material used. In addition, scaled-down physical model tests on reinforced flexible pavement structure were performed by Thaisri (2007) (Section 2.4.2.2). The results of this study were similar to the results of Laurinavičius and Oginskas (2006). When considering the footing settlement, it was found that the permanent deformation of AC layer decreased when reinforced with geosynthetic (Figure 2.22). Then, the maximum shear strain distribution of the based layer was uniformly distributed with the average value that was lower than the one when unreinforced (Figure 2.23).

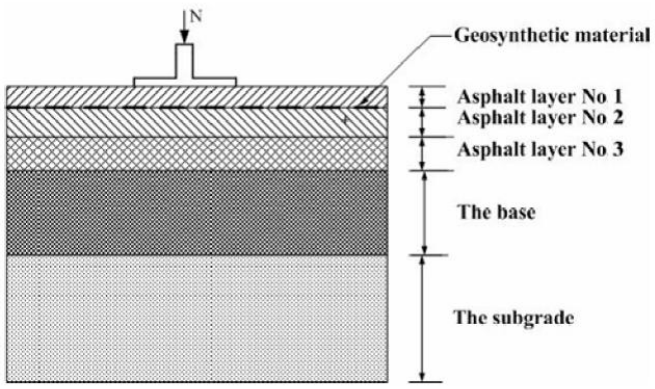

Figure 2.21 Geosynthetic-reinforced pavement research scheme (Laurinavičius and Oginskas, 2006)

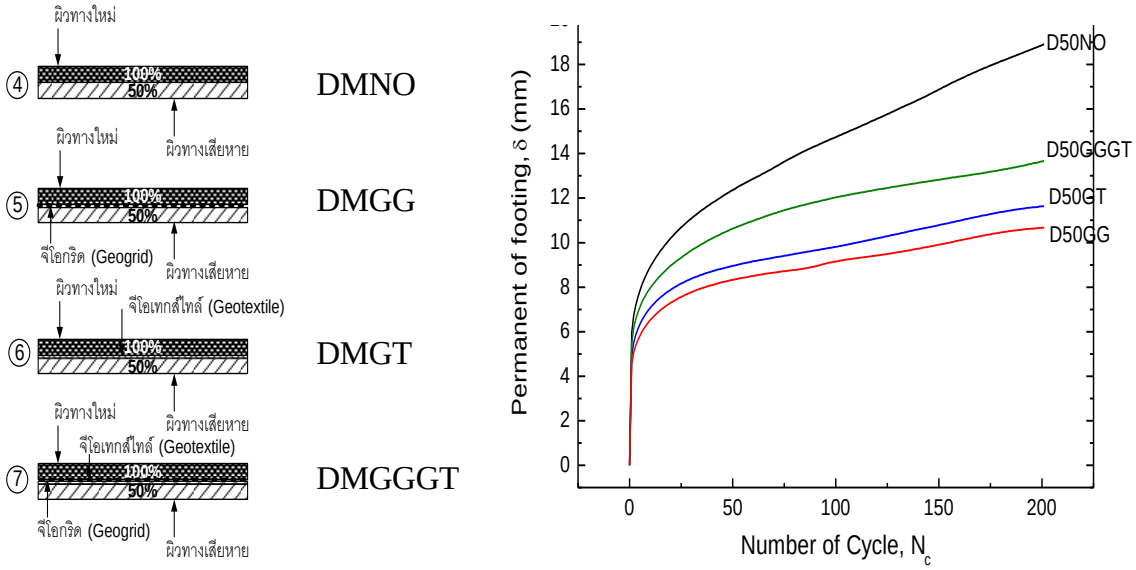

Figure 2.22 Number of cycle-Permanent settlement Relationships of Overlayed Unreinforced and Reinforced Asphalt Concrete Pavement (Thaisri, 2007)

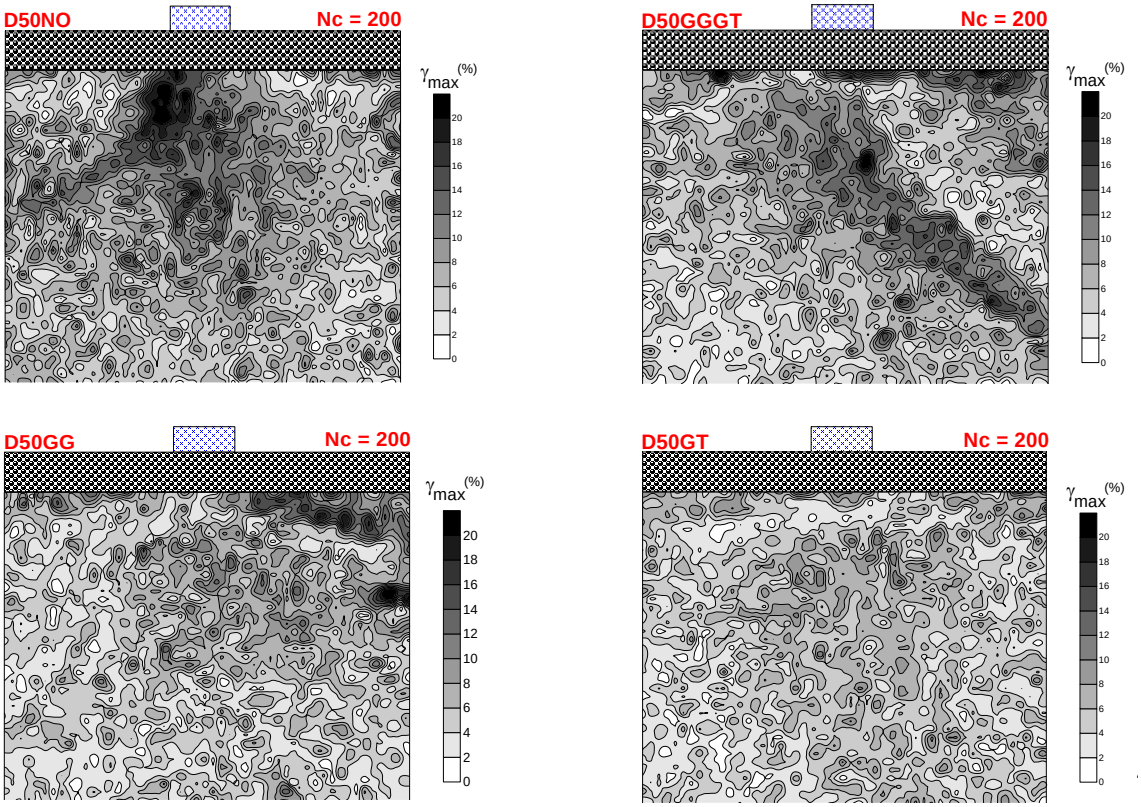

Figure 2.23 Strain fields of Overlayed Unreinforced and Reinforced Asphalt Concrete Pavement (Thaisri, 2007)

Fatigue tests of overlayed reinforced pavement were investigated in the airfield at Imam Khomeini airport, Tehran (Hosseini et al., 2009). Non-reinforced, reinforced with a geogrid and geotextile specimens with dimensions of 50x63x381 mm were obtained from the asphalt slab field section and were tested with a four point beam test. The results indicated that specimens reinforced with geosynthetics have improved stability and integrity compared to non-reinforced specimens. Moreover, the widths of the cracks are decreased.

In the field test, multiple end-to-end test pavements incorporating geosynthetic products (fabrics, grids, and composites) and including control sections were constructed in three different regions of Texas (Amarillo, Waco, and Pharr Districts) (Chowdhury et al., 2009). Performance of these test pavements has been monitored for five to six years, depending on the date of construction. The oldest test pavements (Pharr) are exhibiting essentially no cracking. The Amarillo and Waco test pavements are exhibiting a fair amount of low severity and a very small amount of medium-severity reflective cracking. Usually, for the first couple of years, geosynthetic products perform somewhat better than the control section.

2.5.3 Effect of Location of Geosynthetics in HMA Overlays Pavement

An experimental program was conducted to determine the effects of position of geosynthetic reinforcement on mitigating reflection cracking in asphalt overlays (Khodaii et al., 2009). The layered pavement structure, which was used in this study, was consisted of an asphalt overlayed, which may be unreinforced or reinforced at any depth (embedded at the bottom, the middle and the one-third from the bottom of asphalt

overlayed), a block of asphalt or concrete, simulating discontinuous existing pavements (depth 100 mm) and a resilient subgrade modeled with neoprene rubber. Cyclic square loads were applied to the top center of the beam through a circular loading plate, which was placed on the top of asphalt overlayed. Then, the result between permanent deformation and cycle of loading showed in Figure 2.24. The geosynthetics, was embedded at one-third from the bottom of asphalt overlayed, showed a less permanent deformation when compared at the same cycle.

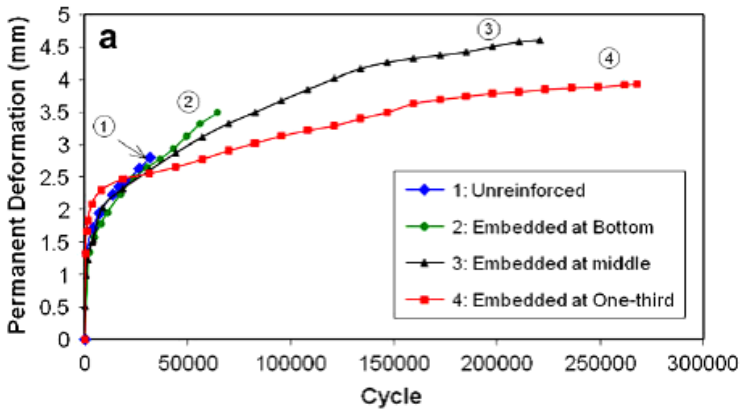

Figure 2.24 Permanent deformation for overlays with an asphalt block base and 10 mm gap at 20 °C (Khodaii et al., 2009)

2.6 Strain Fields from Photogrametric Analysis

A photogrametric analysis was used to investigate the shear band formation in a granular material. This analysis focuses on measurements of the strain lacalization outside and inside the shear bands (Kongkitkul, 2004).

2.6.1 Method to Obtain Coordinates

A latex rubber membrane with a number of printed markers was attached with acrylic confining platen (Kongkitkul, 2004), as shown in Figure 2.25. One mm-head maker pen having black colour with rapidly dried sustainable ink, was used to draw the markers. The shape of maker was round and diameter of each marker was about 1 mm. In addition, the reference points, which stayed stationary during the test, were printed on the frame of the acrylic confining platen. Then, the photos of latex rubber membrane were taken by using a 5 Mega pixel digital camera through the acrylic confining platen during each test.

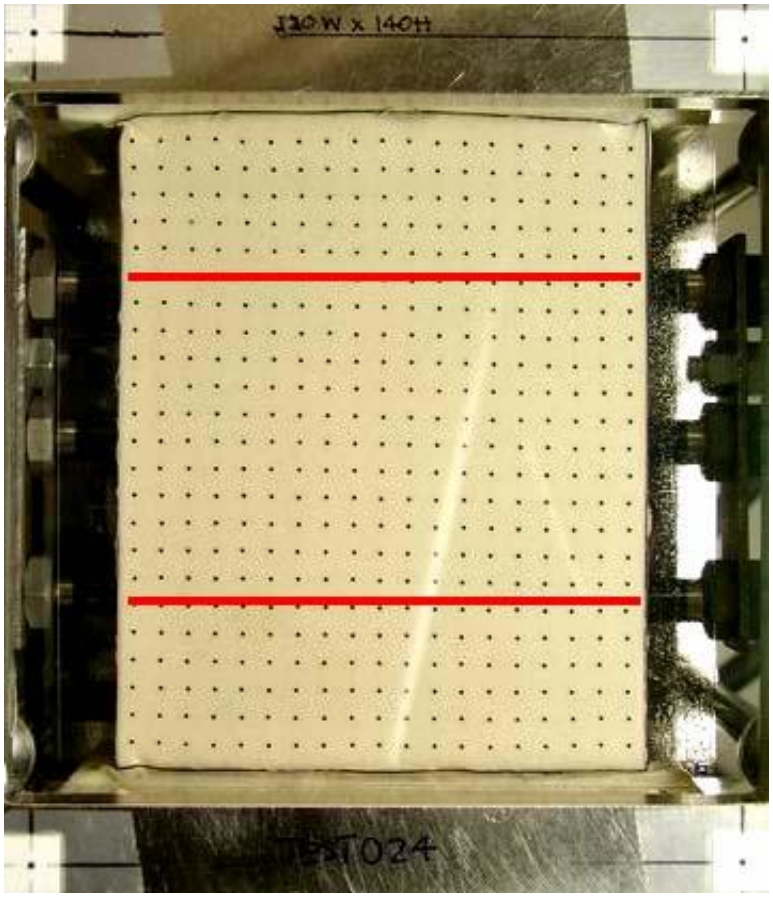

Figure 2.25 A latex rubber membrane with a number of printed markers and the four reference markers (Kongkitkul, 2004)

The taken photos were converted from colour to be black and white and were printed out with a high-resolution ink-jet printer on a sheet of photo-quality super high-grade colour paper. A machine (Figure 2.26) was used to automatically read the coordinates (x, y) of each marker. Nowadays, the digitising software (Figure 2.27) was used to read coordinates (x, y) of markers.

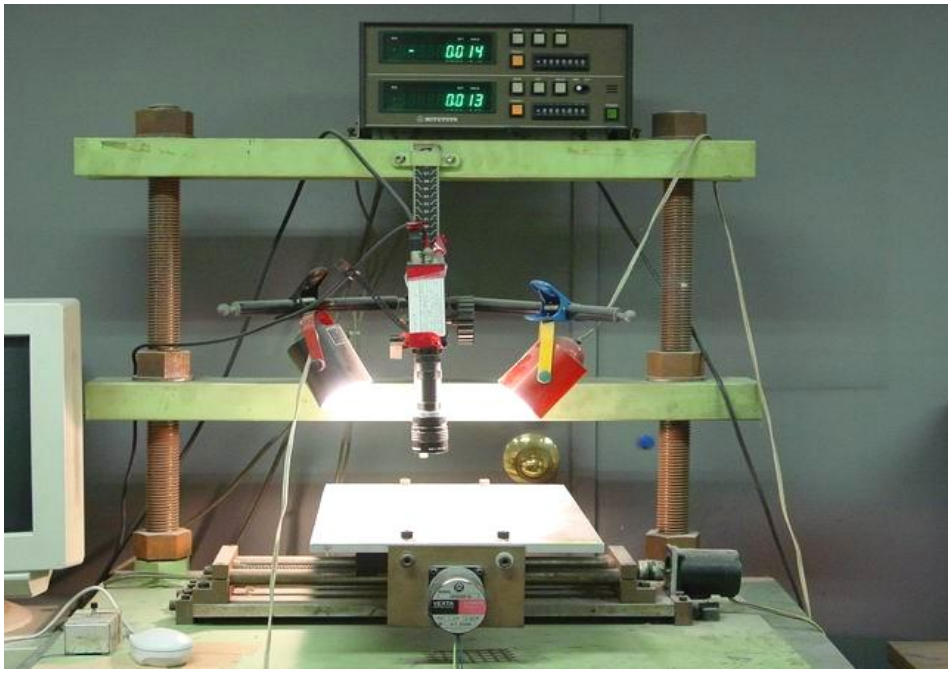

Figure 2.26 Machine to digitise the coordinates of markers on taken photo placed on movable table equipped with high accuracy servo motor (Kongkitkul, 2004)

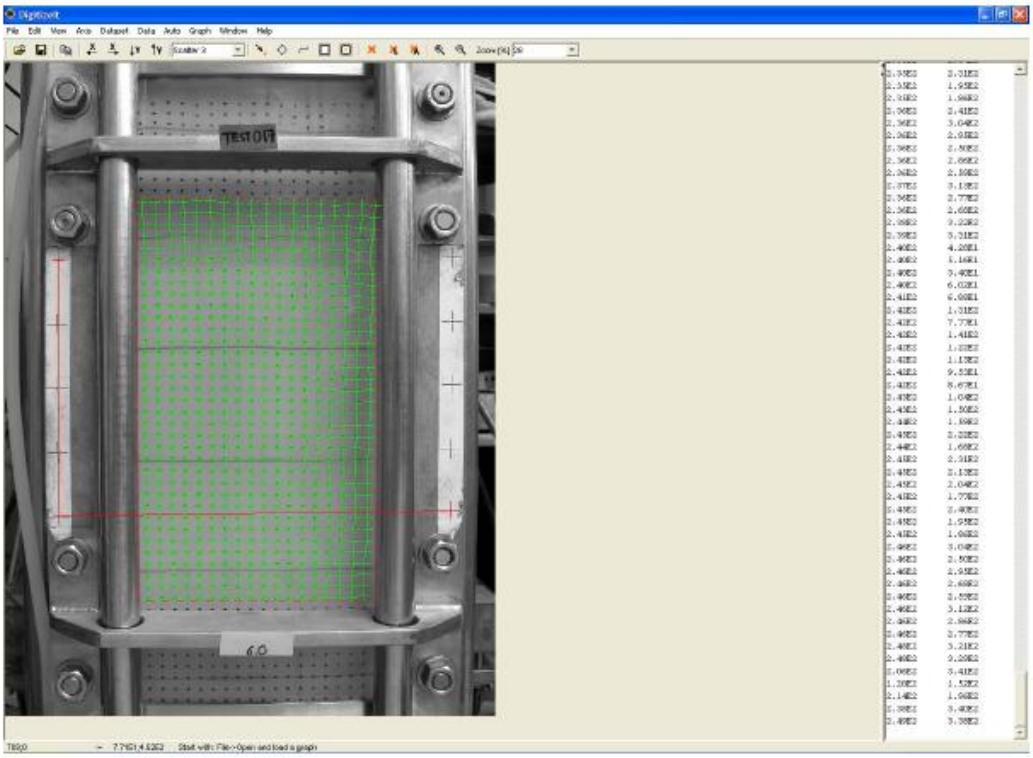

Figure 2.27 Digitising software (Kongkitkul, 2009)

2.6.2 Calculation of Strain Fields

After having finished digitizing and correcting the coordinates of photos for each respective test, a calculation of strain for elements can be done by using isoparametric formulation. Referring to Figure 2.25, the plane bilinear isoparametric elements was used to calculate the strain field values. Isoparametric coordinates in a plane are shown in Figure 2.28(a).

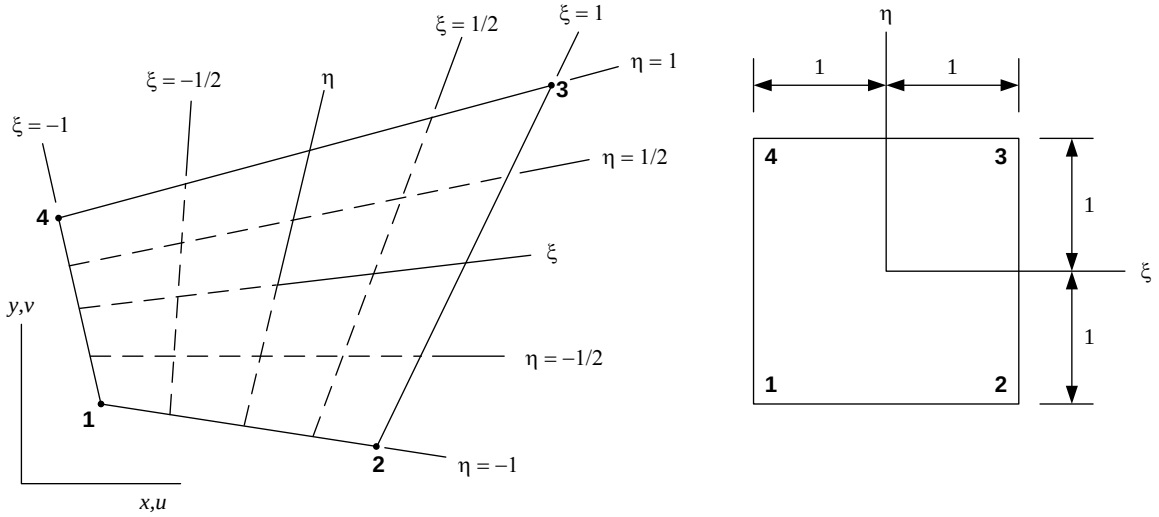

(a) (b)

Figure 2.28 (a) Four-node plane isoparametric element in *xy* space (Cartesian coordinate system) and (b) Plane isoparametric element in $\xi\eta$ space (Natural coordinate system) (Kongkitkul, 2004)

Coordinates of each node forming the four-node plane element must be transformed from Cartesian system (obtained from digitizing machine or software) to natural system (local). For a single four-node element, the local coordinate (ξ,η) of any point within an element can be mapped or transformed to global Cartesian coordinates (x,y) by:

$$x(\xi,\eta)=\sum_{i=1}^{4} N_i(\xi,\eta)\cdot x_i \tag{2.2a}$$

$$y(\xi,\eta)=\sum_{i=1}^{4} N_i(\xi,\eta)\cdot y_i \tag{2.2b}$$

where: (x_i,y_i) = Cartesian coordinates of each of four nodes

$N_i(\xi,\eta)$ = Shape function, which is defined as:

$$N_i(\xi,\eta)=\frac{1}{4}(1+\xi_i\cdot\xi)(1+\eta_i\cdot\eta) \tag{2.3}$$

where: (ξ_i, η_i) = The coordinates of the respective four nodes in the natural coordinate system. Consequently, the followings can be derived:

$$N_1(\xi,\eta) = \frac{1}{4}(1-\xi)(1-\eta) \tag{2.4a}$$

$$N_2(\xi,\eta) = \frac{1}{4}(1+\xi)(1-\eta) \tag{2.4b}$$

$$N_3(\xi,\eta) = \frac{1}{4}(1+\xi)(1+\eta) \tag{2.4c}$$

$$N_4(\xi,\eta) = \frac{1}{4}(1-\xi)(1+\eta) \tag{2.4d}$$

Strain fields are calculated in terms of a field variable ϕ and its derivatives $\partial\phi/\partial x$ and $\partial\phi/\partial y$. For strain analysis, the field variables ϕ are displacement scalars u and v in x and y directions, respectively.

For isoparametric elements, the shape function representing the field variables and the one representing geometries (coordinates) are identical. Consequently, any field variable can be expressed by using the same shape function as follows:

$$\phi(\xi,\eta) = \sum_{i=1}^{4} N_i(\xi,\eta)\cdot\phi_i \tag{2.5}$$

and its derivative with respect to x and y is given as follows:

$$\frac{\partial\phi}{\partial x} = \sum_{i=1}^{4} \frac{\partial N_i}{\partial x}\cdot\phi_i \tag{2.6a}$$

$$\frac{\partial\phi}{\partial y} = \sum_{i=1}^{4} \frac{\partial N_i}{\partial y}\cdot\phi_i \tag{2.6b}$$

For example, the local displacement scalars $u(\xi,\eta)$ and $v(\xi,\eta)$ of any point within the element, referring to Equation 2.5, can be expressed as:

$$u(\xi,\eta) = \sum_{i=1}^{4} N_i(\xi,\eta)\cdot u_i \qquad (x\text{-direction})$$

$$v(\xi,\eta) = \sum_{i=1}^{4} N_i(\xi,\eta)\cdot v_i \qquad (y\text{-direction})$$

However, the results of derivative of the shape function with respect to x and y cannot directly be determined. By using Chain rule, the derivative of the shape function with respect to ξ and η can be expressed as follows:

$$\frac{\partial N_i}{\partial \xi} = \frac{\partial N_i}{\partial x} \cdot \frac{\partial x}{\partial \xi} + \frac{\partial N_i}{\partial y} \cdot \frac{\partial y}{\partial \xi} \tag{2.7a}$$

$$\frac{\partial N_i}{\partial \eta} = \frac{\partial N_i}{\partial x} \cdot \frac{\partial x}{\partial \eta} + \frac{\partial N_i}{\partial y} \cdot \frac{\partial y}{\partial \eta} \tag{2.7b}$$

These two above equations can be written in matrix form as:

$$\begin{bmatrix} \frac{\partial N_i}{\partial \xi} \\ \frac{\partial N_i}{\partial \eta} \end{bmatrix} = \begin{bmatrix} \frac{\partial x}{\partial \xi} & \frac{\partial y}{\partial \xi} \\ \frac{\partial x}{\partial \eta} & \frac{\partial y}{\partial \eta} \end{bmatrix} \begin{bmatrix} \frac{\partial N_i}{\partial x} \\ \frac{\partial N_i}{\partial y} \end{bmatrix} = [J] \begin{bmatrix} \frac{\partial N_i}{\partial x} \\ \frac{\partial N_i}{\partial y} \end{bmatrix} \tag{2.7bis}$$

where: $[J]$ = Jacobian matrix.

At this moment, the derivatives of the shape function with respect to x and y can be determined by using the inverse of the Jacobian matrix as follows:

$$\begin{bmatrix} \frac{\partial N_i}{\partial x} \\ \frac{\partial N_i}{\partial y} \end{bmatrix} = [J]^{-1} \begin{bmatrix} \frac{\partial N_i}{\partial \xi} \\ \frac{\partial N_i}{\partial \eta} \end{bmatrix} \tag{2.8}$$

Subsequently, the inverse of the Jacobian matrix can be expressed as:

$$[J]^{-1} = \frac{1}{|J|} \begin{bmatrix} J_{22} & -J_{12} \\ -J_{21} & J_{11} \end{bmatrix} \tag{2.9}$$

where: $|J| = J_{11} \cdot J_{22} - J_{12} \cdot J_{21}$ is the determinant of the Jacobian matrix.

From now, the derivative of the shape function with respective to x and y as shown in Equation 2.8 can be re-written as follows:

$$\begin{bmatrix} \frac{\partial N_i}{\partial x} \\ \frac{\partial N_i}{\partial y} \end{bmatrix} = \frac{1}{|J|} \begin{bmatrix} J_{22} & -J_{12} \\ -J_{21} & J_{11} \end{bmatrix} \begin{bmatrix} \frac{\partial N_i}{\partial \xi} \\ \frac{\partial N_i}{\partial \eta} \end{bmatrix} \tag{2.10}$$

In this study, strains were calculated at the center of each element where (ξ, η) = $(0,0)$. Consequently, the following derivative results can be obtained:

$$\frac{\partial N_1}{\partial \xi} = -\frac{1}{4}(1-\eta) = -\frac{1}{4} \qquad \frac{\partial N_1}{\partial \eta} = -\frac{1}{4}(1-\xi) = -\frac{1}{4}$$

$$\frac{\partial N_2}{\partial \xi} = \frac{1}{4}(1-\eta) = \frac{1}{4} \qquad \frac{\partial N_2}{\partial \eta} = -\frac{1}{4}(1+\xi) = -\frac{1}{4}$$

$$\frac{\partial N_3}{\partial \xi} = \frac{1}{4}(1+\eta) = \frac{1}{4} \qquad \frac{\partial N_3}{\partial \eta} = \frac{1}{4}(1+\xi) = \frac{1}{4} \tag{2.11}$$

$$\frac{\partial N_4}{\partial \xi} = -\frac{1}{4}(1+\eta) = -\frac{1}{4} \qquad \frac{\partial N_4}{\partial \eta} = \frac{1}{4}(1-\xi) = \frac{1}{4}$$

Consequently, each member of the Jacobian matrix can be determined as follows:

$$J_{11} = \frac{\partial x}{\partial \xi} = \sum_{i=1}^{4} \frac{\partial N_i}{\partial \xi} \cdot x_i = \frac{1}{4}(-x_1 + x_2 + x_3 - x_4)$$

$$J_{12} = \frac{\partial y}{\partial \xi} = \sum_{i=1}^{4} \frac{\partial N_i}{\partial \xi} \cdot y_i = \frac{1}{4}(-y_1 + y_2 + y_3 - y_4)$$

$$J_{21} = \frac{\partial x}{\partial \eta} = \sum_{i=1}^{4} \frac{\partial N_i}{\partial \eta} \cdot x_i = \frac{1}{4}(-x_1 - x_2 + x_3 + x_4) \tag{2.12}$$

$$J_{22} = \frac{\partial y}{\partial \eta} = \sum_{i=1}^{4} \frac{\partial N_i}{\partial \eta} \cdot y_i = \frac{1}{4}(-y_1 - y_2 + y_3 + y_4)$$

Subsequently, the derivatives of the shape function with respect to x and y can be expressed in more details as follows:

$$\frac{\partial N_1}{\partial x} = \frac{1}{|J|} \cdot \left[J_{22} \cdot \frac{\partial N_1}{\partial \xi} - J_{12} \cdot \frac{\partial N_1}{\partial \eta} \right] = \frac{1}{|J|} \cdot \left[-\frac{1}{4} \cdot J_{22} + \frac{1}{4} \cdot J_{12} \right]$$

$$\frac{\partial N_2}{\partial x} = \frac{1}{|J|} \cdot \left[J_{22} \cdot \frac{\partial N_2}{\partial \xi} - J_{12} \cdot \frac{\partial N_2}{\partial \eta} \right] = \frac{1}{|J|} \cdot \left[\frac{1}{4} \cdot J_{22} + \frac{1}{4} \cdot J_{12} \right]$$

$$\frac{\partial N_3}{\partial x} = \frac{1}{|J|} \cdot \left[J_{22} \cdot \frac{\partial N_3}{\partial \xi} - J_{12} \cdot \frac{\partial N_3}{\partial \eta} \right] = \frac{1}{|J|} \cdot \left[\frac{1}{4} \cdot J_{22} - \frac{1}{4} \cdot J_{12} \right] \tag{2.13a}$$

$$\frac{\partial N_4}{\partial x} = \frac{1}{|J|} \cdot \left[J_{22} \cdot \frac{\partial N_4}{\partial \xi} - J_{12} \cdot \frac{\partial N_4}{\partial \eta} \right] = \frac{1}{|J|} \cdot \left[-\frac{1}{4} \cdot J_{22} - \frac{1}{4} \cdot J_{12} \right]$$

and

$$\frac{\partial N_1}{\partial y} = \frac{1}{|J|} \cdot \left[-J_{21} \cdot \frac{\partial N_1}{\partial \xi} + J_{11} \cdot \frac{\partial N_1}{\partial \eta} \right] = \frac{1}{|J|} \cdot \left[\frac{1}{4} \cdot J_{21} - \frac{1}{4} \cdot J_{11} \right]$$

$$\frac{\partial N_2}{\partial y} = \frac{1}{|J|} \cdot \left[-J_{21} \cdot \frac{\partial N_2}{\partial \xi} + J_{11} \cdot \frac{\partial N_2}{\partial \eta} \right] = \frac{1}{|J|} \cdot \left[-\frac{1}{4} \cdot J_{21} - \frac{1}{4} \cdot J_{11} \right]$$

$$\frac{\partial N_3}{\partial y} = \frac{1}{|J|} \cdot \left[-J_{21} \cdot \frac{\partial N_3}{\partial \xi} + J_{11} \cdot \frac{\partial N_3}{\partial \eta} \right] = \frac{1}{|J|} \cdot \left[-\frac{1}{4} \cdot J_{21} + \frac{1}{4} \cdot J_{11} \right] \quad (2.13b)$$

$$\frac{\partial N_4}{\partial y} = \frac{1}{|J|} \cdot \left[-J_{21} \cdot \frac{\partial N_4}{\partial \xi} + J_{11} \cdot \frac{\partial N_4}{\partial \eta} \right] = \frac{1}{|J|} \cdot \left[\frac{1}{4} \cdot J_{21} + \frac{1}{4} \cdot J_{11} \right]$$

By the known coordinates x and y at the four nodes of each element, the Jacobian matrix of the respective element can be determined by following Equation 2.12. Subsequently, the derivatives of the shape function with respect to x and y can be calculated by following Equation 2.13.

2.6.4 Calculation of Strain Values

In order to calculate the strain values of the respective element, it is necessary to determine the values of the displacements at each nodes i, (i = 1, 2, 3, 4) (Figure 2.29). The displacement scalars u and v were calculated as:

$$u_i = x_i - (x_i)_{initial} \quad (2.14a)$$

$$v_i = y_i - (y_i)_{initial} \quad (2.14b)$$

where: (x_i, y_i) = The coordinates of node i at an instant t

$(x_i, y_i)_{initial}$ = The coordinates of node i at the start of testing.

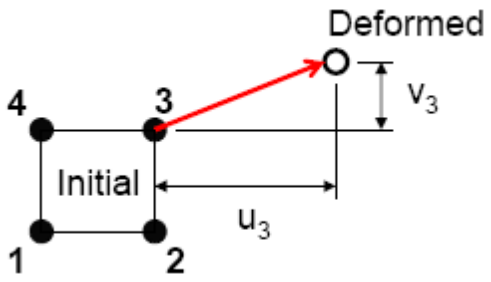

Figure 2.29 Values of the displacements at nodes i = 3 (Kongkitkul, 2009)

Following the continuum theory, the following equations are derived to calculate the values of strain:

Horizontal strain (positive for compression):

$$\varepsilon_x = -\frac{\partial u}{\partial x} = -\sum_{i=1}^{4} \frac{\partial N_i(\xi,\eta)}{\partial x} \cdot u_i \tag{2.15}$$

$$= -\left[\frac{\partial N_1}{\partial x} \cdot u_1 + \frac{\partial N_2}{\partial x} \cdot u_2 + \frac{\partial N_3}{\partial x} \cdot u_3 + \frac{\partial N_4}{\partial x} \cdot u_4 \right]$$

Vertical strain (positive for compression):

$$\varepsilon_y = -\frac{\partial v}{\partial y} = -\sum_{i=1}^{4} \frac{\partial N_i(\xi,\eta)}{\partial y} \cdot v_i \tag{2.16}$$

$$= -\left[\frac{\partial N_1}{\partial y} \cdot v_1 + \frac{\partial N_2}{\partial y} \cdot v_2 + \frac{\partial N_3}{\partial y} \cdot v_3 + \frac{\partial N_4}{\partial y} \cdot v_4 \right]$$

Shear strain:

$$\gamma_{xy} = -\left[\frac{\partial u}{\partial y} + \frac{\partial v}{\partial x} \right] = -\left[\sum_{i=1}^{4} \frac{\partial N_i(\xi,\eta)}{\partial y} \cdot u_i + \sum_{i=1}^{4} \frac{\partial N_i(\xi,\eta)}{\partial x} \cdot v_i \right] \tag{2.17}$$

$$= -\left[\frac{\partial N_1}{\partial y} \cdot u_1 + \frac{\partial N_2}{\partial y} \cdot u_2 + \frac{\partial N_3}{\partial y} \cdot u_3 + \frac{\partial N_4}{\partial y} \cdot u_4 + \frac{\partial N_1}{\partial x} \cdot v_1 + \frac{\partial N_2}{\partial x} \cdot v_2 + \frac{\partial N_3}{\partial x} \cdot v_3 + \frac{\partial N_4}{\partial x} \cdot v_4 \right]$$

Major principal strain:

$$\varepsilon_1 = \frac{1}{2}\left(\varepsilon_x + \varepsilon_y\right) + \sqrt{\frac{1}{4}\left(\varepsilon_x - \varepsilon_y\right)^2 + \left(\frac{\gamma_{xy}}{2}\right)^2} \tag{2.18}$$

Minor principal strain:

$$\varepsilon_3 = \frac{1}{2}\left(\varepsilon_x + \varepsilon_y\right) - \sqrt{\frac{1}{4}\left(\varepsilon_x - \varepsilon_y\right)^2 + \left(\frac{\gamma_{xy}}{2}\right)^2} \tag{2.19}$$

Maximum shear strain:

$$\gamma_{\max} = \varepsilon_1 - \varepsilon_3 \tag{2.20}$$

Volumetric strain (positive for compression; n.b., $\varepsilon_2 \equiv 0$***):***

$$\varepsilon_{vol} = \varepsilon_1 + \varepsilon_3 \tag{2.21}$$

For calculating these strain values, source codes were newly written in MATLAB computer program. Three sets of source codes were written considering the different patterns of arrangement of element. Subsequently, the strain contours were plotted by using Surfer program (Figure 2.30).

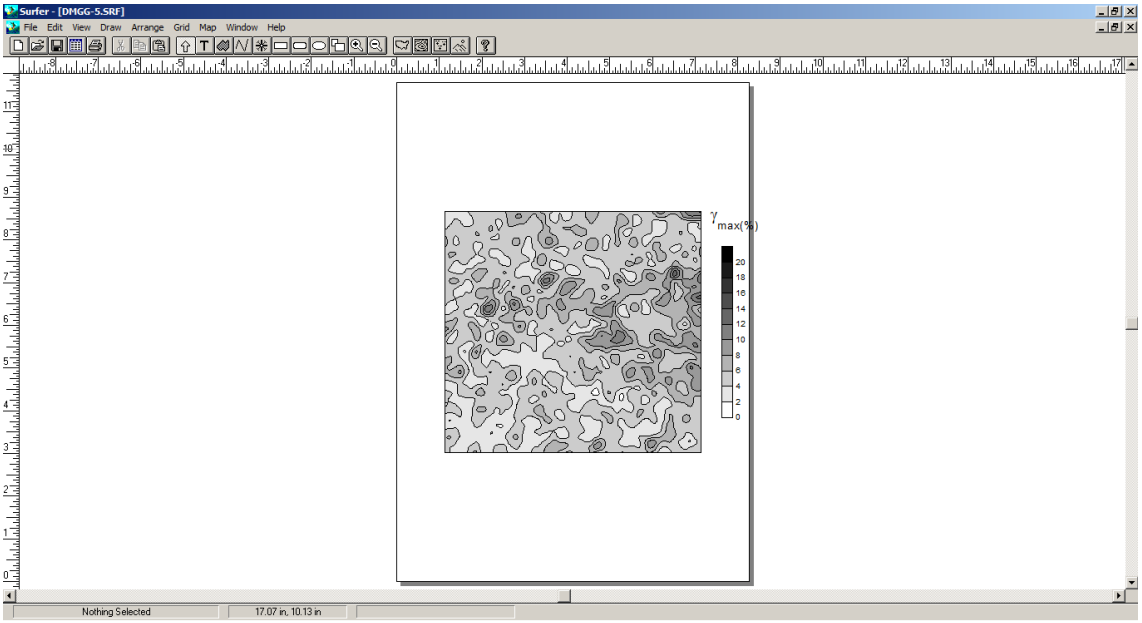

Figure 2.30 Surfer software

2.6.5 Formulations of Element

There were three types of element implemented by Kongkitkul (2004). The descriptions are following:

Normal elements: This kind of element is the most basic one as shown in Figure 2.31(a). Each element was constructed without any overlapping. In this study, the numbers of marker in the vertical and horizontal directions are 48and 19 52, respectively. Consequently, the numbers of "normal element" are (48-1) = 47 and (52-1) = 51 in the vertical and horizontal directions, respectively. As depicted in Figure 2.31(a), at element, '*p+2*', the coordinates (x, y) and displacement scalars u and v of this element were calculated from the four surrounding coordinates to form the element: '2m+3', '2m+2', 'm+2' and 'm+3'.

Normal overlapping elements: This kind of element is similar to the "normal element". Each 'normal overlapping element' was formed by the four nodes arranged to have a size of about 10 mm x 10 mm, as shown in Figure 2.31(b) (Kongkitkul, 2004). The elements were overlapping normal elements in both vertical and horizontal directions. Thus, the numbers of "normal overlapping element" are (48-2) = 46 and (52-2) = 50 in the vertical and horizontal directions, respectively. The strain values of respective element were calculated from the displacement scalars u and v that were

calculated from the coordinates of the four nodes forming the 'normal overlapping element'. For example, as shown in Figure 2.31(b), at the "normal overlapping element", 's+2', the coordinates (x, y) and displacement scalars u and v of this element were calculated from the four surrounding coordinates to form the element: '3m+4', '3m+2', 'm+2' and 'm+4'.

Directly average overlapping elements: This kind of element, combining the two above methods, determines the coordinates and strain values of each respective element. That is, the coordinates of the "directly average overlapping element" is the same as the ones of the "normal overlapping element". However, the strain values of the respective "directly average overlapping element" is obtained by directly averaging the strain values of the inside four "normal elements". For example, as shown in Figure 2.31(c), at "directly average overlapping element", 's+2', the coordinates (x, y) of this element were determined from the four surrounding coordinates to form the element: '3m+4', '3m+2', 'm+2' and 'm+4'. However, the strain values of this element were calculated by directly averaging the strain values of the inside four "normal elements": '*2p+3*', '*2p+2*', '*p+2*' and '*p+3*'. The strain values of other directly average overlapping elements together with the respective element coordinates were calculated by using the algorithm described above.

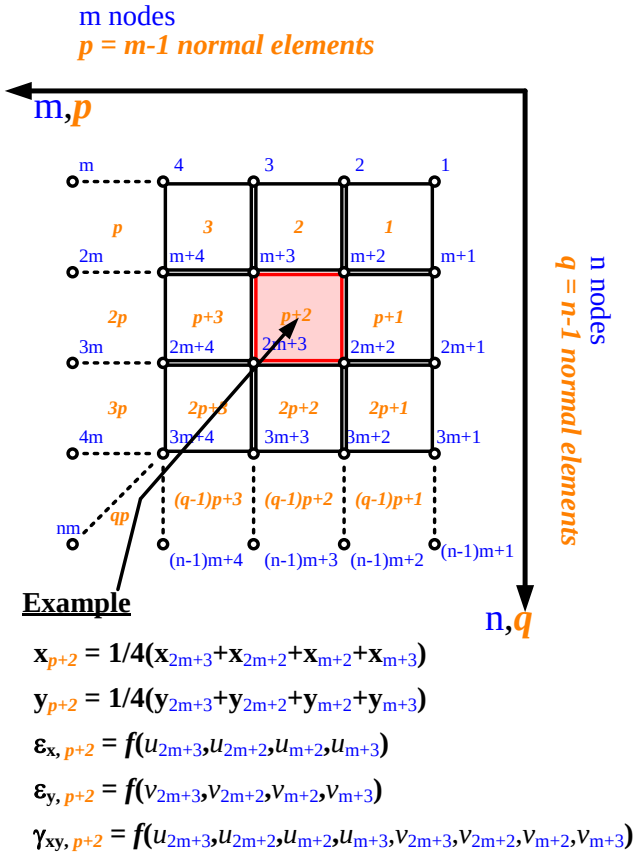

Figure 2.31(a) Diagram showing how to obtain the coordinates and the strain values by using "normal element" (Kongkitkul, 2004)

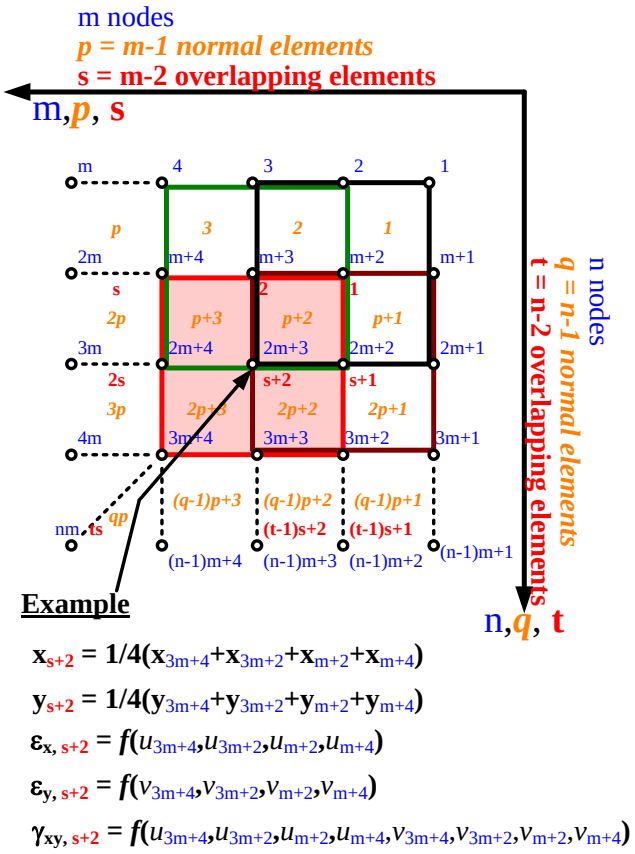

Figure 2.31(b) Diagram showing how to obtain the coordinates and the strain values by using "normal overlapping element" (Kongkitkul, 2004)

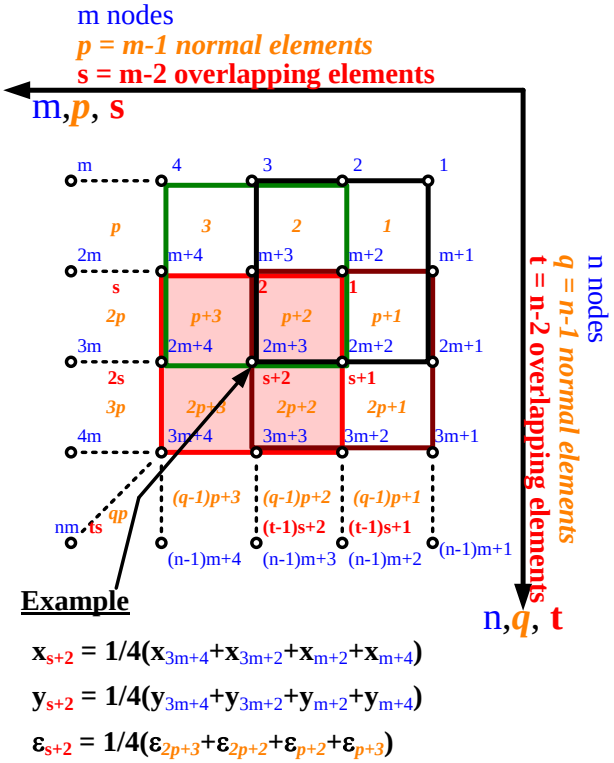

Figure 2.31(c) Diagram showing how to obtain the coordinates and the strain values by using "directly average overlapping element" (Kongkitkul, 2004)